CHAPTER IV
RESULTS AND DISCUSSION

4.1 Precursors Synthesis and Characterizations

Generally, zeolites are synthesized from freshly prepared sodium aluminosilicate gel, from various silica and alumina sources by hydrothermal treatment. In this work, the Oxide-One-Pot-Synthesis (OOPS) process, silatrane and alumatrane were successfully synthesized from silica (SiO_2) and alumina (Al_2O_3) under an inert atmosphere. By-products generated from the condensation reaction were also continuously removed from the system by the inert gas purging. The synthesized products were washed with dry acetonitrile to remove non-reacting triethanolamine (TEA), triisopropanolamine (TIS) and ethylene glycol (EG). Subsequently, the purified products were reserved under vacuum to avoid the hydrolysis process that rapidly executes by absorbed moisture.

4.1.1 Silatrane Characterizations

Synthesized silatrane was characterized by using FTIR and Thermogravimetric analysis (TGA) as shown in Table 4.1 and Figures 4.1-4.2, respectively.

Table 4.1 Peak positions and assignments in the FTIR spectrum of synthesized silatrane

Peak positions (cm^{-1})	Assignments
3100-3700	ν(O–H)
2800-3000	ν(C–H)
1445, 1459, 1500	δ(C–H)
1351	ν(C–N)
1276, 1022	ν(C–O)
1080-1180, 1049	ν(Si–O)
1096	ν(Si–O–C)
700-940	δ(Si–O–C)
580	Si← N

The IR spectrum (Figure 4.1) also clearly evidences the success of silatrane synthesis since almost identical characteristic peaks reported by Phiriyawirut *et al.*, 2003 and Sathupanya *et al.*, 2003 were observed.

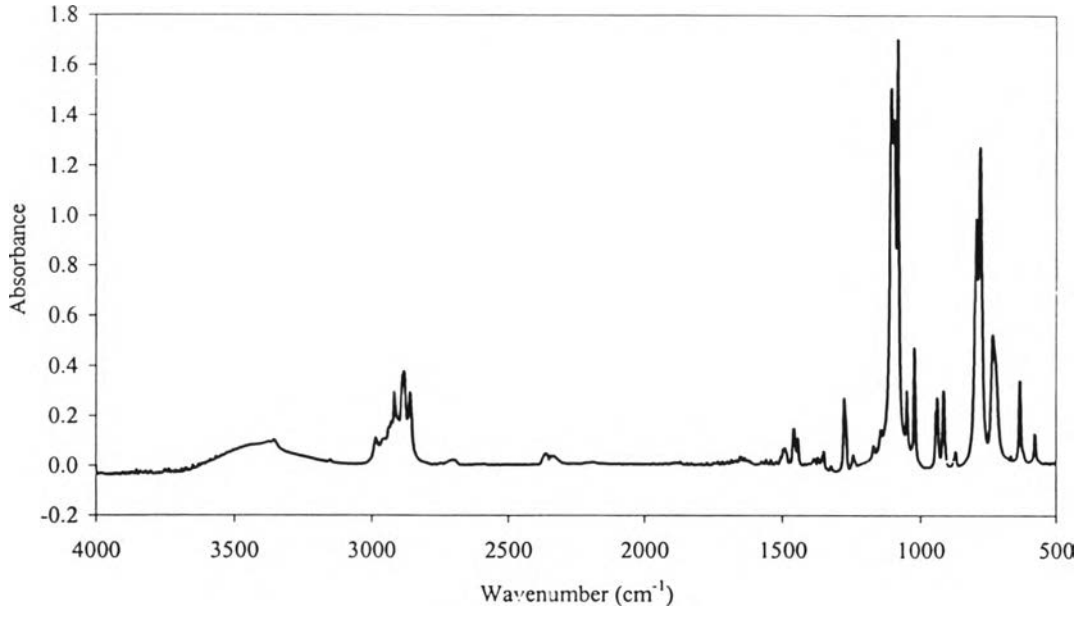

Figure 4.1 FTIR spectrum of silatrane.

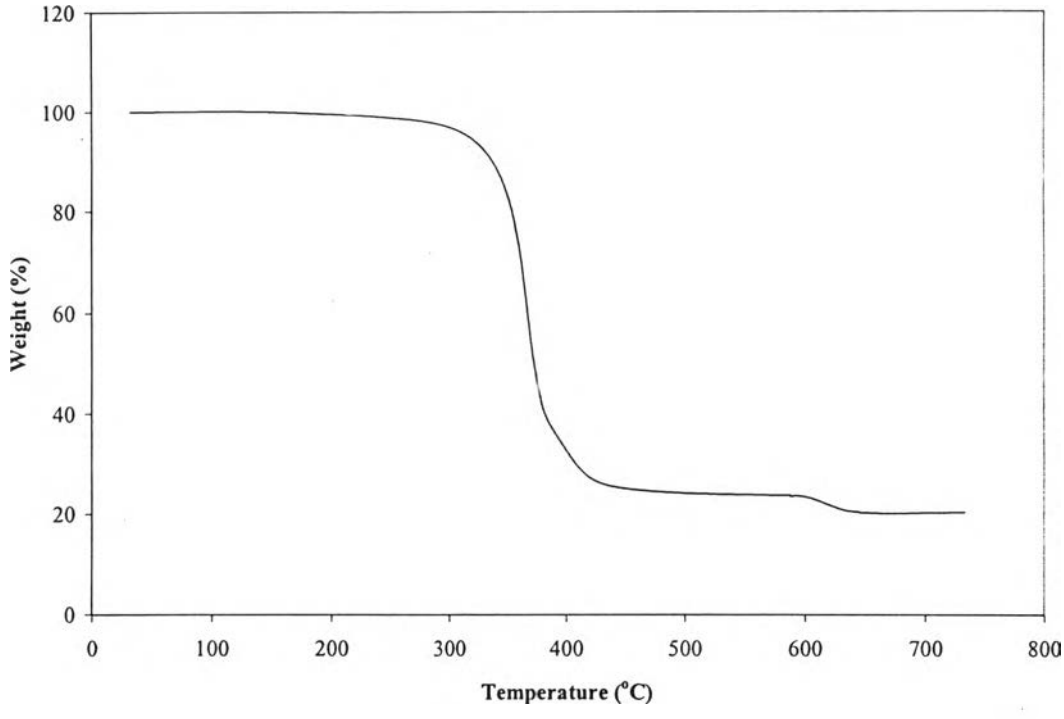

Figure 4.2 TGA thermogram of silatrane.

The TGA thermogram of the purified product, as illustrated in Figure 4.2, reveals two mass loss transitions, the first mass loss at 300-450°C corresponding to the organic ligand oxidation, and the other is at 590-620°C corresponding to the residue carbon char oxidation. The residue mass of 20.2% also indicates the ceramic yield of the product, which is slightly higher than the theoretical value reported in literature (Phiriyawirut *et al.*, 2003 and Sathupanya *et al.*, 2003).

From both FTIR and TGA results, it was obviously indicated that the synthesized product is a desired silatrane (Si-TEA), and confidentially to be used as zeolite precursor.

4.1.2 Alumatrane Characterizations

Figure 4.3 illustrates the FTIR spectrum of alumatrane, which has the characteristic peaks as shown in Table 4.2.

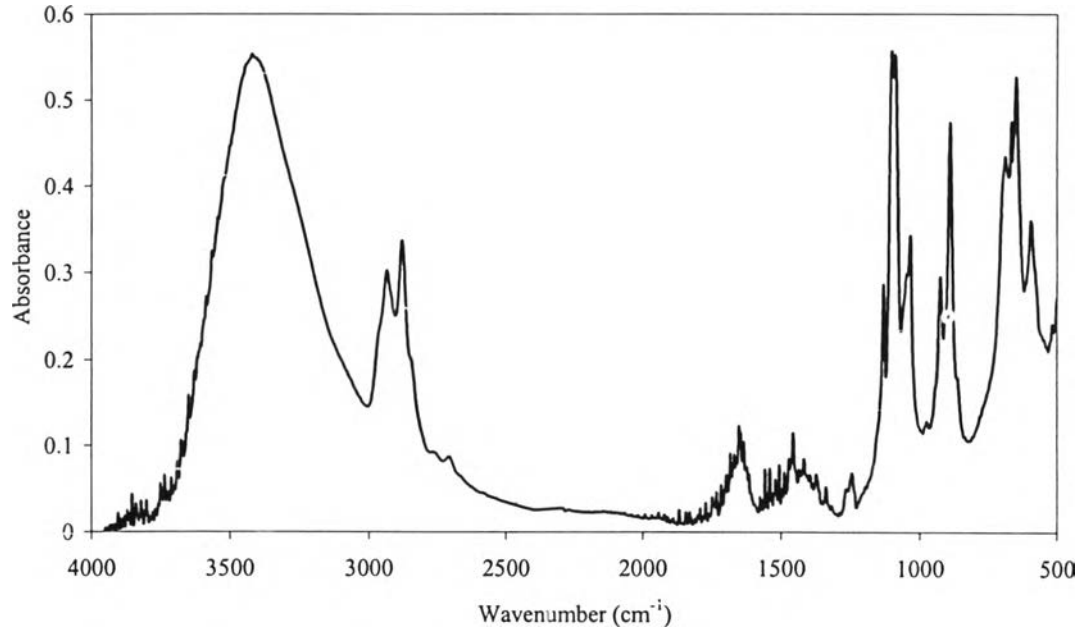

Figure 4.3 FTIR spectrum of alumatrane.

Table 4.2 Peak positions and assignments in the FTIR spectrum of synthesized alumatrane

Peak positions (cm^{-1})	Assignments
3100-3700	ν(O–H)
2800-3000	ν(C–H)
1653	O–H overtone
1457	δ(C–H)
1133	ν(C–O)
1030-1100	ν(Al–O–C)
900-1000	ν(C–N)
890	δ(Al–O–C)
500-800	ν(Al–O)

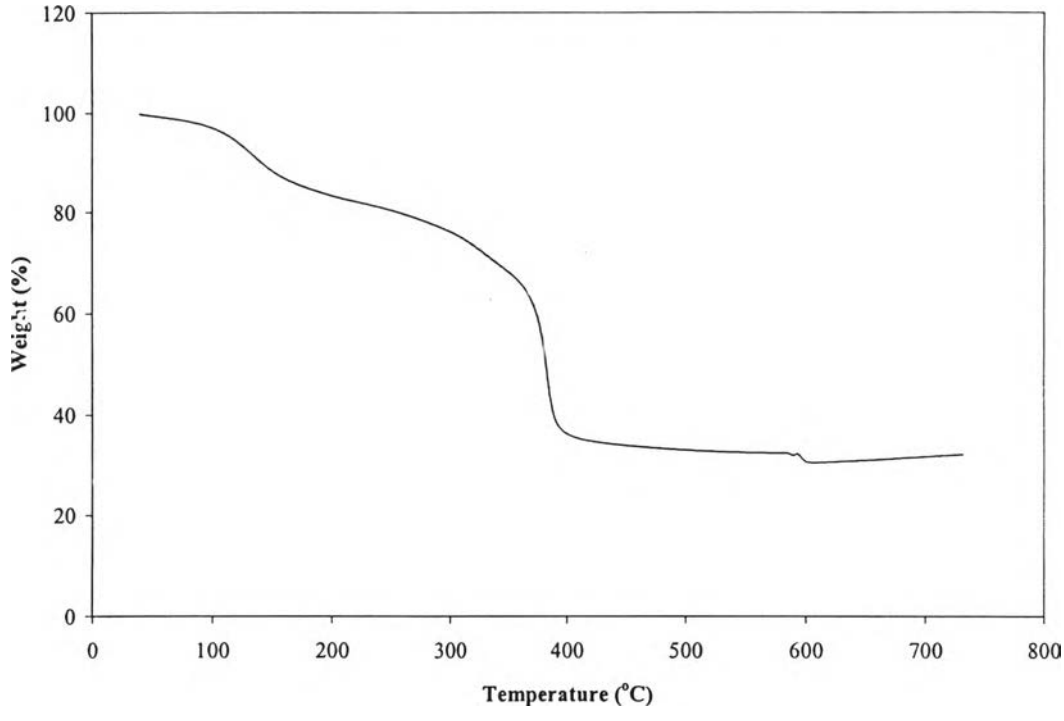

Figure 4.4 TGA thermogram of alumatrane.

The TGA result (Figure 4.4) with three mass loss regions, 50-200°C of trapped solvent and TIS decomposition, 200-550°C of organic ligand decomposition and 580-600°C of residual carbon char oxidation, also gives a good agreement with the previously reported results of alumatrane and also indicates 32.6% of ceramic yield of synthesized product that is higher than the theoretical value reported in literature (Phiriyawirut *et al.*, 2003 and Sathupanya *et al.*, 2003).

Therefore, both FTIR and TGA results confirm that the synthesized product is alumatrane (Al-TIS) and can be used as a zeolite precursor.

4.2 KH Zeolite Synthesis and Characterizations

4.2.1 Single Batch Synthesis

KH zeolites were synthesized by sol-gel process using Si-TEA and Al-TIS as precursors and KOH as the hydrolytic agent. The Si-TEA and Al-TIS was mixed with KOH solution at room temperature with a fixed molar ratio of SiO_2:

$0.1Al_2O_3$: $3K_2O$: $410H_2O$. The gel mixture was aged for 12 hrs before undergoing hydrothermal microwave treatment at 150°C for 5 hrs (Sathupanya *et al.*, 2004). The XRD pattern and SEM micrographs of single batch synthesized KH zeolite are shown in Figures 4.5 and 4.6, respectively.

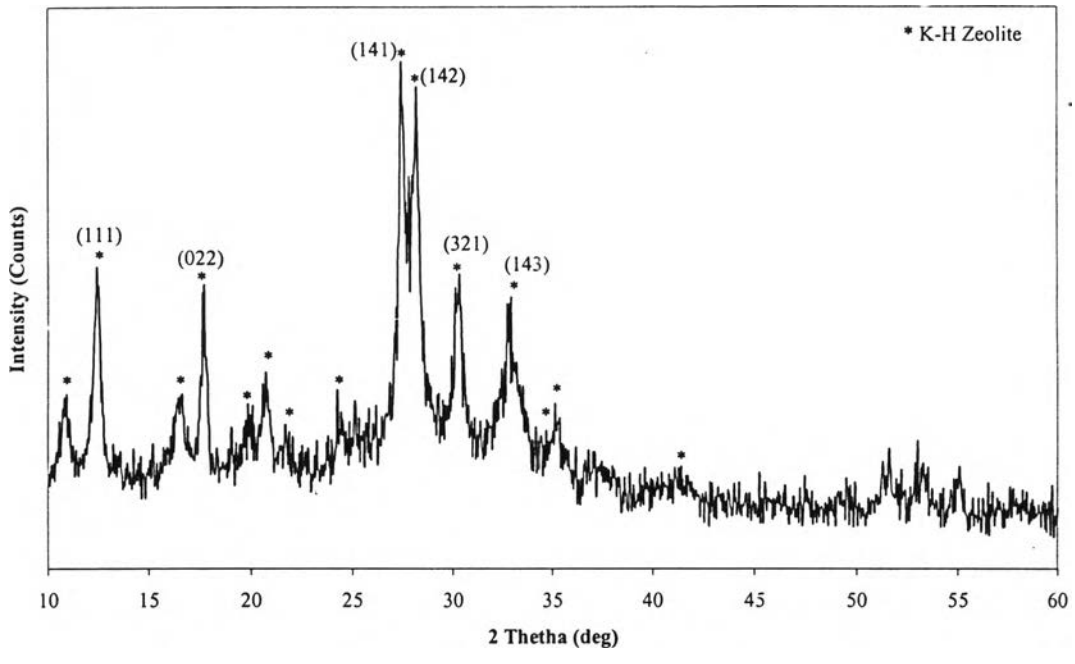

Figure 4.5 XRD pattern of single batch KH zeolite synthesized from SiO_2:$0.1Al_2O_3$:$3K_2O$:$410H_2O$ of 150°C and 5 hrs hydrothermal conditions.

The XRD pattern of the synthesized KH zeolite closely matches that of KH zeolite ($K_2Al_2Si_4O_{12}.xH_2O$) in the literature (Sathupanya *et al.*, 2004 and Mimura *et al.*, 2001). It is apparent that the XRD pattern consists of 15 main reflections corresponding to (111), (022), (141), (142), (321) and (143) planes. The SEM micrographs also indicate the flower-shape and dog-bone shape of synthesized KH zeolite with diameter of around 13 μm closely to the result of Sathupanya *et al.*, (2004). Therefore, it appears that KH zeolite was successfully synthesized in this single batch scale.

Generally, many parameters including temperature, time and pH play important roles influence the crystal morphology and size. Thus, in this work the reaction temperature and time were fixed at the optimum condition of 150°C and 5 hrs, respectively.

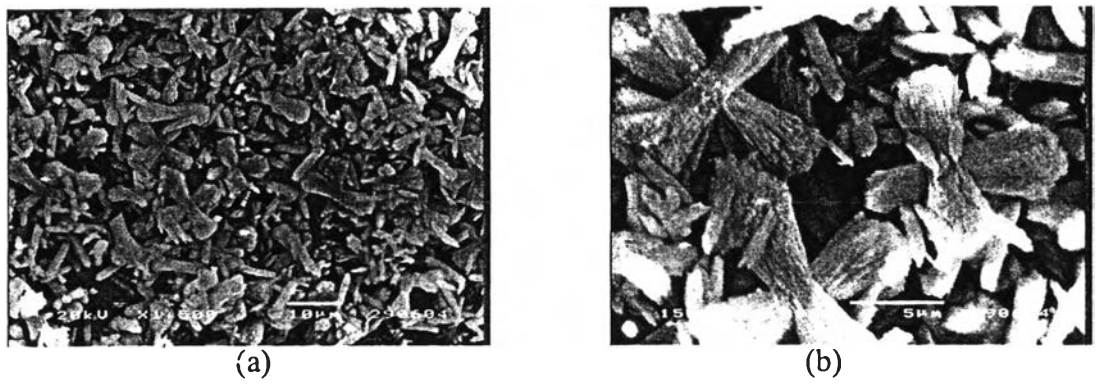

(a) (b)

Figure 4.6 SEM micrographs of single batch KH zeolite synthesized from SiO_2:0.1Al_2O_3:3K_2O:410H_2O of 150°C and 5 hrs hydrothermal conditions at magnification: (a) 1500 and (b) 5000.

4.2.1.1 Effect of KOH Concentrations

The SiO_2:K_2O ratios were varied from 1:1 5 to 1:3 while keeping all the other parameters constant at a ratio of SiO_2:0.1Al_2O_3:410H_2O with 16 hrs gelation time at 150°C and 5 hrs hydrothermal conditions. The XRD patterns of synthesized products, as illustrated in Figure 4.7, show that the main KH zeolite reflections appeared only when above 1:2 of SiO_2:K_2O ratios were used. This result indicates that KH zeolite can be successfully synthesized when using SiO_2:K_2O ratios above 1:2.

SEM micrographs of the synthesized products obtained from the single batch scale synthesis after hydrothermal microwave treatment are shown in Figure 4.8. The micrographs obviously illustrated the morphology differences of the different SiO_2:K_2O ratios synthesized products. Therefore, it can be concluded that the concentration of KOH also has an effect on both crystallinity and morphology. Moreover, it was found that the dog-bone shape of synthesized product was increased as the concentration of KOH increased, and those dog-bones were coupled to be a flower-shape like at high KOH concentrations.

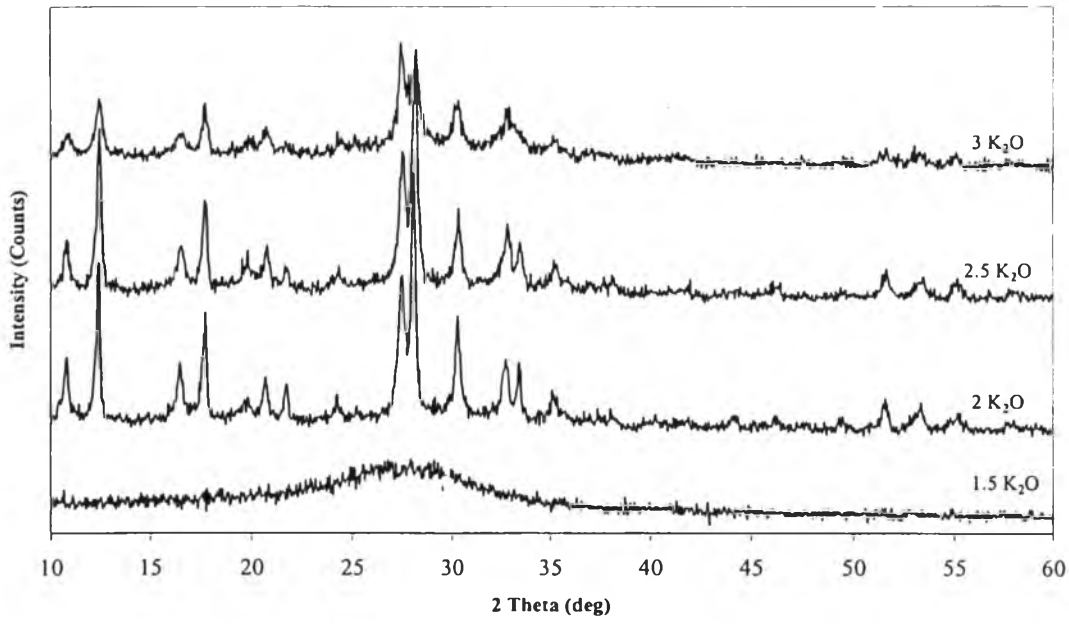

Figure 4.7 XRD patterns of single batch synthesized products obtained from SiO_2:0.1Al_2O_3: ***a*** K_2O:410H_2O (***a*** = 1.5 to 3) at 150°C, 5 hrs.

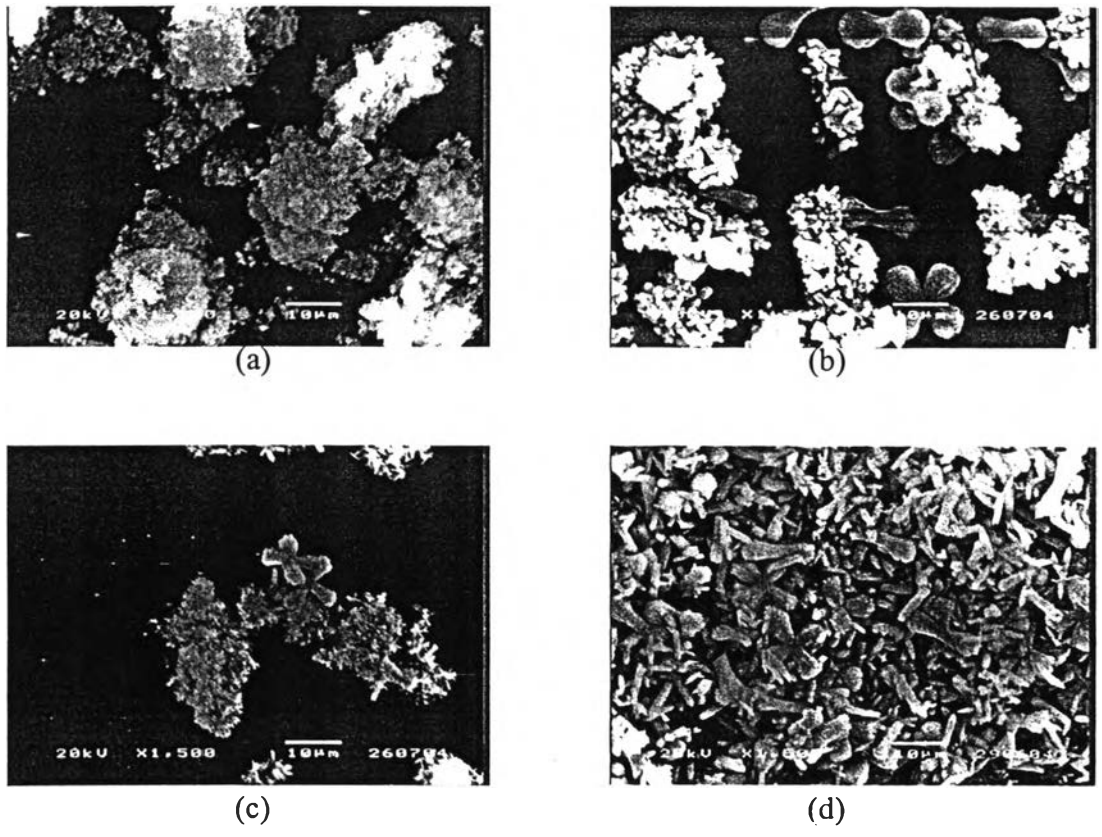

Figure 4.8 SEM micrographs of single batch synthesized products obtained from SiO_2:0.1Al_2O_3: ***a*** K_2O:410H_2O at 150°C, 5 hrs; ***a*** = (a) 1.5, (b) 2, (c) 2.5 and (d) 3.

4.2.1.2 Effect of Crystallization Time

The study was performed under a fixed ratio of SiO_2: $0.1Al_2O_3$: $3K_2O$: $410H_2O$, 22.30 hrs of gelation time and at temperature of 150°C, with various crystallization times. The XRD patterns shown in Figure 4.9 reveal very interesting results about the crystallinity of the synthesized products. By increasing crystallization time, from 4 to 5, 7 and 8 hrs, the crystallinity of synthesized product was increased as expected due to an enough time of precursors to form a zeolite unit and eventually to form a KH zeolite. By contrary, the crystallization time of 6 hrs showed an adverse result since the XRD pattern evidences some broad reflection peaks that would means the low crystallinity of the synthesized product.

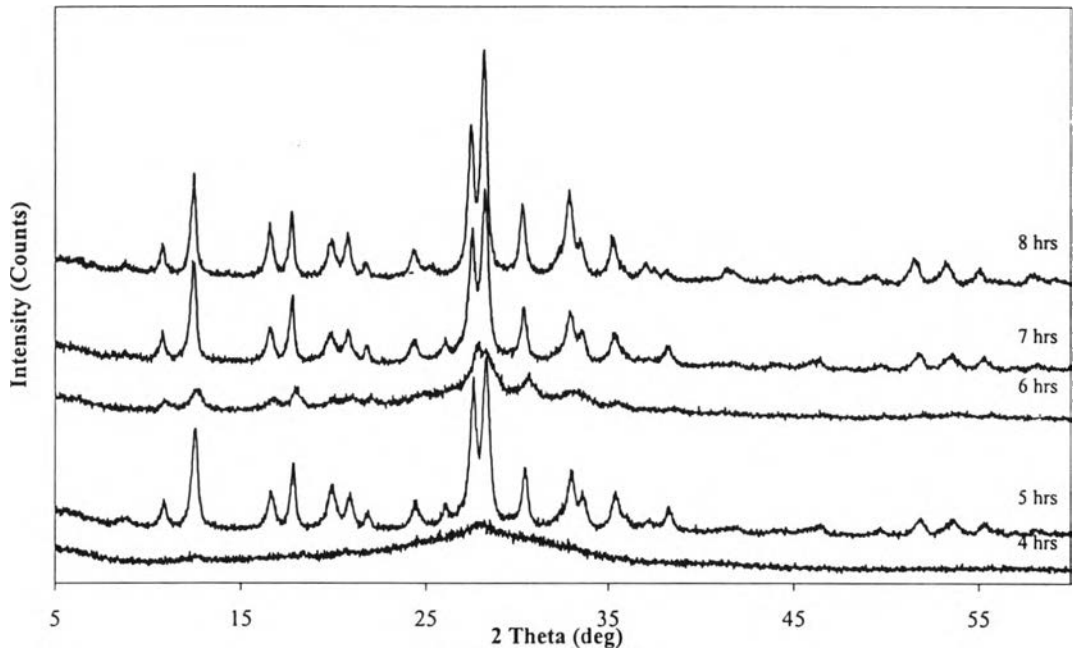

Figure 4.9 XRD patterns of synthesized products obtained with different crystallization time on single batch synthesized products at 150°C. Substrate composition: SiO_2:$0.1Al_2O_3$:$3K_2O$:$410H_2O$; (a) 4, (b) 5, (c) 6, (d) 7 and (e) 8 hrs.

SEM micrographs, as shown in Figure 4.10, also give a good agreement with XRD results. The micrographs show that amorphous material gradually disappeared as the crystallization progressed and the amount of dog-bone

crystalline KH zeolite increased. At the crystallization time of 6 hrs, the amorphous material was also virtually observed in the agreement with the XRD patterns.

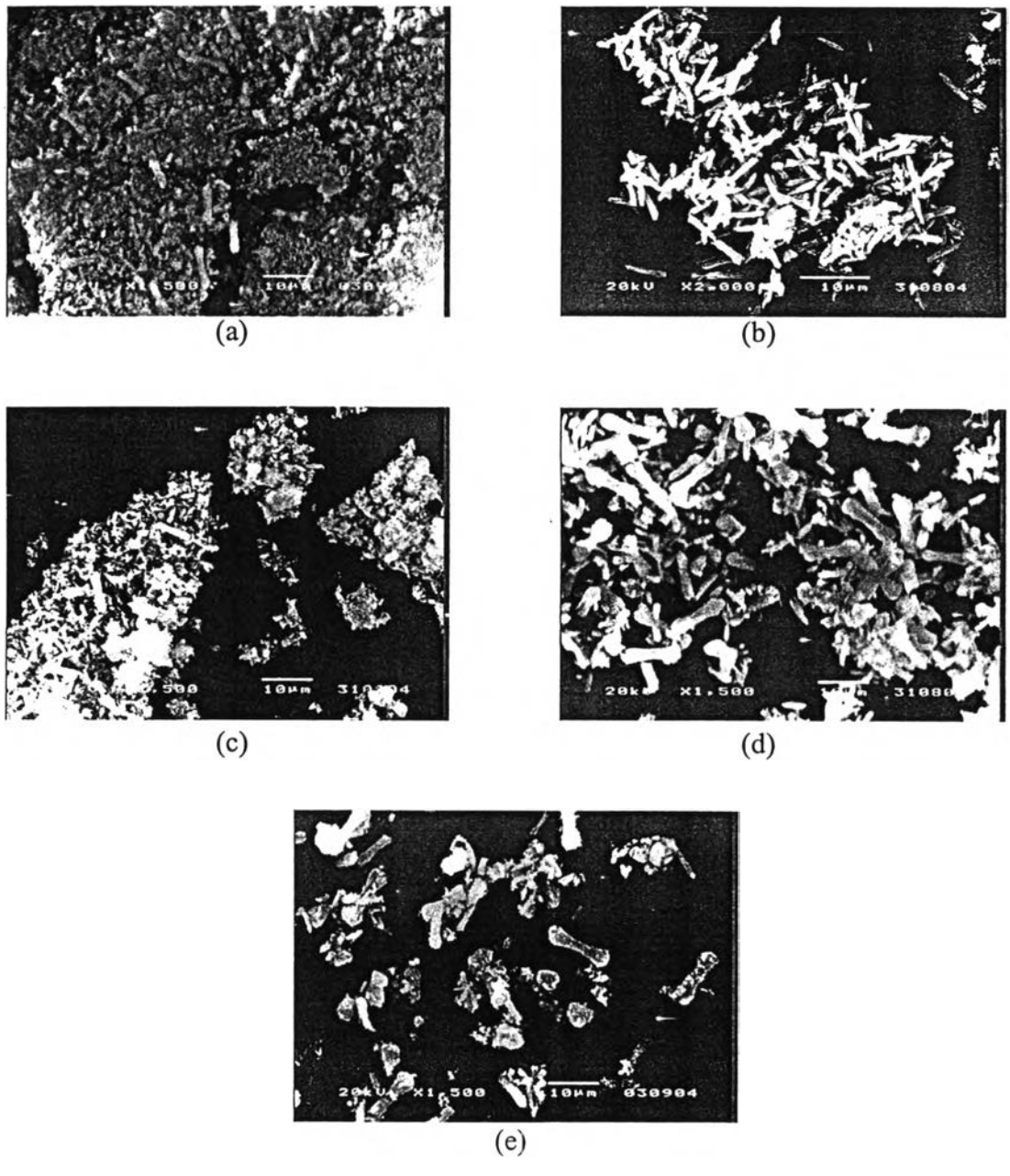

Figure 4.10 SEM micrographs of single batch synthesized products obtained from SiO_2:0.1Al_2O_3: 3K_2O:410H_2O at 150°C and crystallization time of (a) 4, (b) 5, (c) 6, (d) 7 and (e) 8 hrs.

From all single batch scale studies, the peak intensities were observed to develop progressively as the crystallization time increased except at 6 hrs, and the characteristic XRD peaks of KH zeolite began to appear after 4 hrs. KOH concentration and crystallization time are the most important parameters influencing the transformation of the KH zeolites. Fully crystalline KH zeolite was obtained after 8 hrs, but with only 0.1 g of the product. This quantity is not enough and becomes a problem due to an inadequate amount of the zeolite to perform both catalytic activity measurements and characterizations. Therefore, an attempt to obtain more yield of the synthesized KH zeolite was conducted by up scaling from single batch scale to double, triple and quadruple batch scales, respectively.

4.2.2 Double Batch Synthesis

Double batch synthesis was performed at a fixed ratio of $2(SiO_2: 0.1Al_2O_3: 3K_2O: 410H_2O)$ aged for 24 hrs before using hydrothermal microwave treatment at 150°C for 5 hrs.

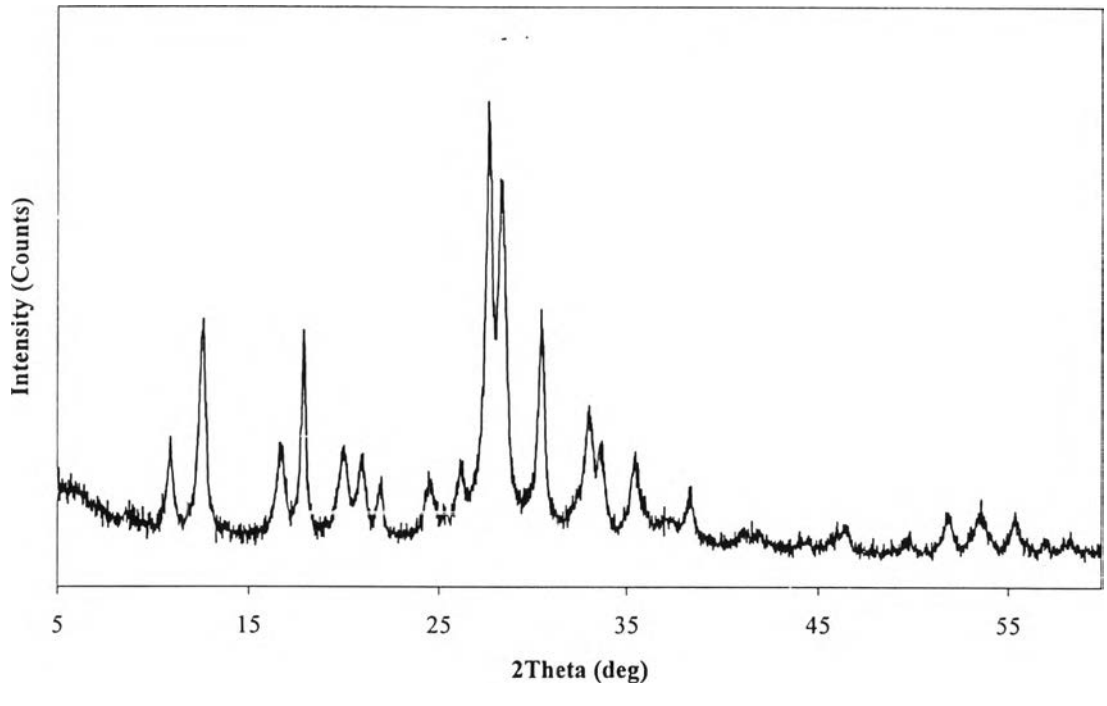

Figure 4.11 XRD pattern of double batch KH zeolite synthesized from $2(SiO_2:0.1Al_2O_3:3K_2O:410H_2O)$), aging for 24 hrs, at 150°C and 5 hrs.

The XRD pattern, as illustrated in Figure 4.11, shows 15 main reflections match to that of KH zeolite. Therefore, this result evidences that under this particular double batch scale condition, KH zeolite can be successfully synthesized. However, the maximum obtained yield was 0.2 g.

SEM micrographs (Figure 4.12) also depict flower-shape and dog-bone morphologies of the double batch scale KH zeolite, but slightly different from that was synthesized in single batch scale.

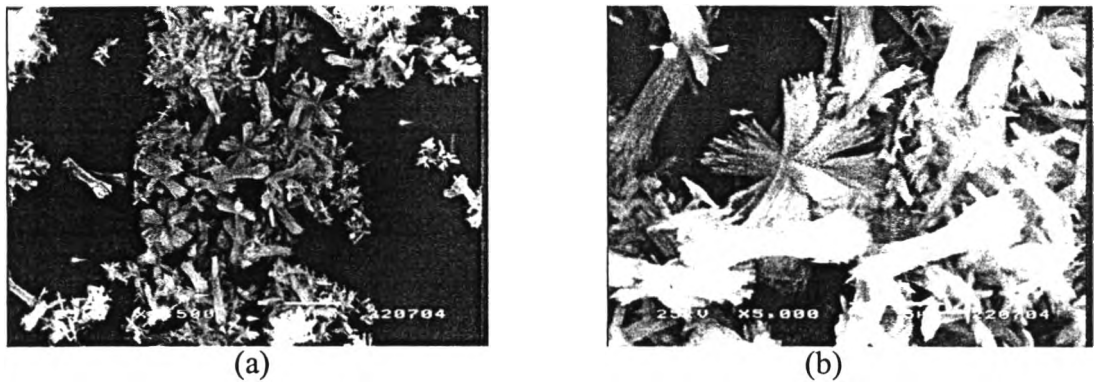

Figure 4.12 SEM micrographs of double batch KH zeolite synthesized from $2(SiO_2{:}0.1Al_2O_3{:}3K_2O{:}410H_2O)$, aging for 24 hrs, at hydrothermal conditions of 150°C and 5 hrs, at magnification: (a) 1500 and (b) 5000.

4.2.3 Triple Batch Synthesis

4.2.3.1 Effect of Gelation Time

For triple batch, the gelation time was studied at a reactant ratio of $3(SiO_2{:}\ 0.1Al_2O_3{:}\ 3K_2O{:}\ 410H_2O)$. The XRD patterns and SEM micrographs of triple batch synthesized product from various gelation times are shown in Figures 4.13 and 4.14, respectively.

The outcomes indicate that gelation time lower than 19 hrs is not sufficient for synthesized KH zeolite at this reactant ratio. On the other hand, the gelation time of 48 hrs was found to be only the appropriate time for triple scale KH zeolite synthesis.

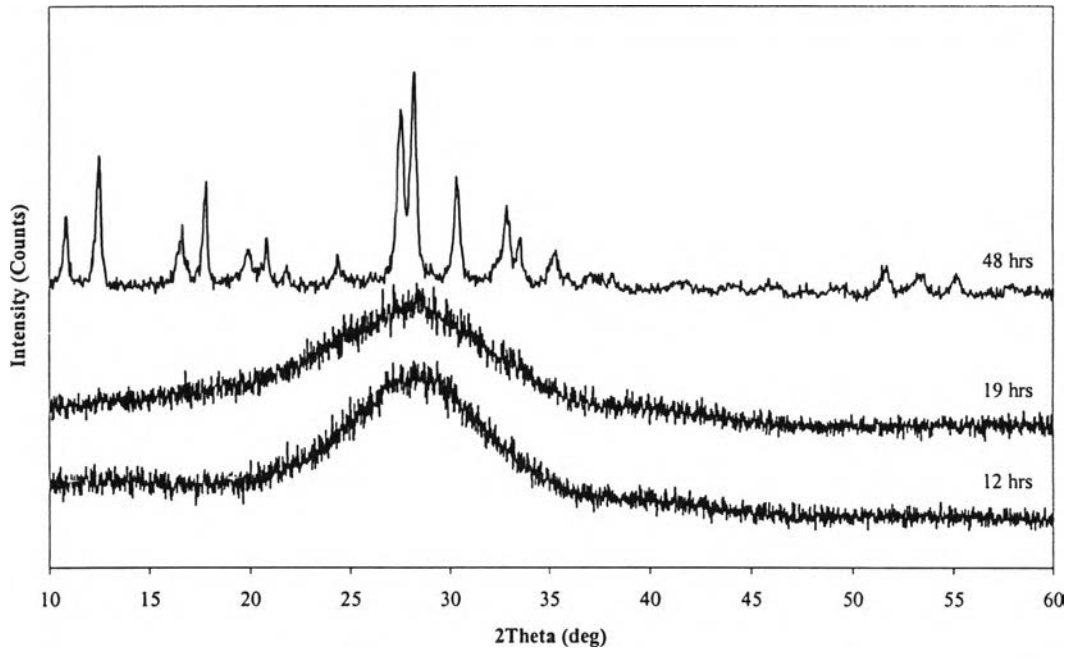

Figure 4.13 XRD patterns of triple batch synthesized products from $3(SiO_2:0.1Al_2O_3:3K_2O:410H_2O)$, aging for ***a*** hrs (***a*** = 12, 19 and 48 hrs), at hydrothermal conditions 150°C and 5 hrs.

Interestingly, the morphologies of all triple batch synthesized products are almost the same which is disorder-shape, even only the product obtained at 48 hrs of gelation time is KH zeolite while the others are amorphous. Therefore, it can be concluded that the up scaling to triple batch can yield KH zeolite as single and double batches, but with the different morphologies and the higher yield. The maximum obtained yield of KH zeolite from this triple batch scale is 0.3 g.

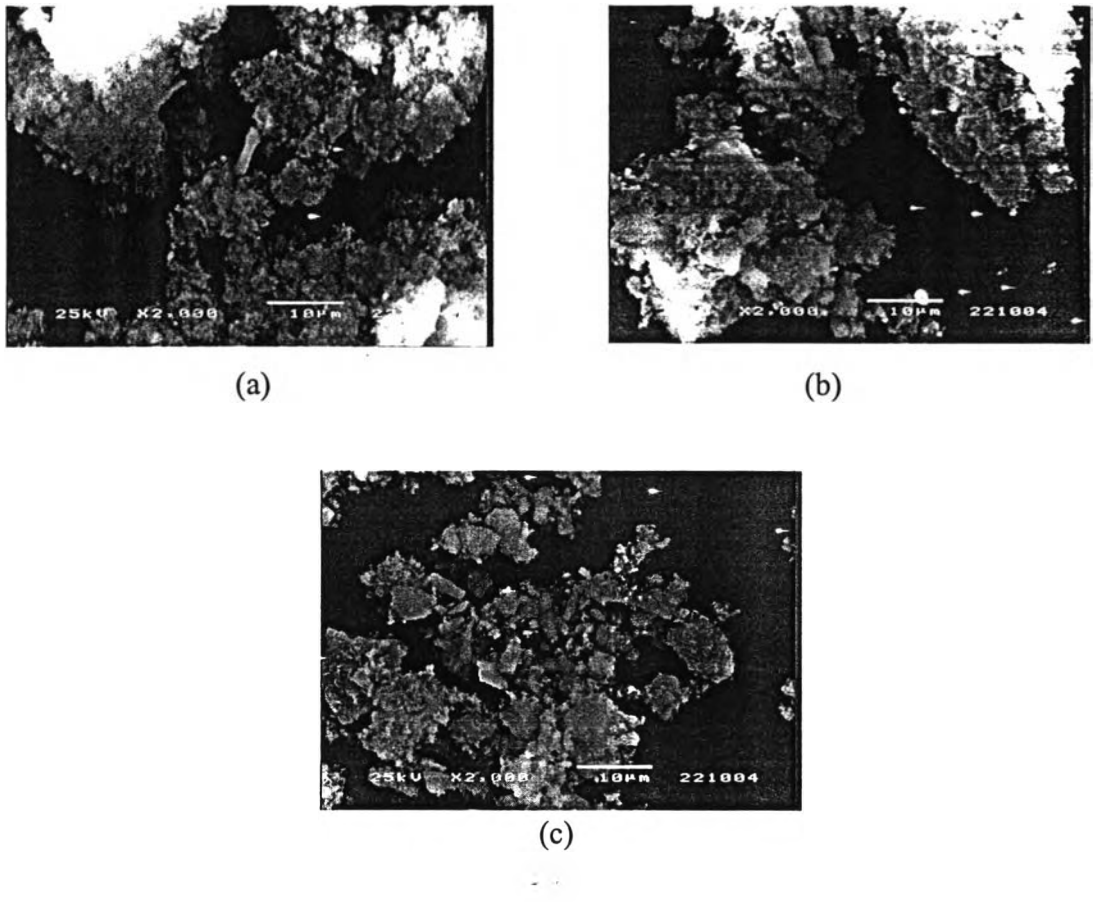

Figure 4.14 SEM micrographs of triple batch synthesized products from $3(SiO_2{:}0.1Al_2O_3{:}\ 3K_2O{:}410H_2O)$ at hydrothermal conditions 150°C and 5 hrs, aging for (a) 12, (b) 19 and (c) 48 hrs.

4.2.4 Quadruple Batch Synthesis

4.2.4.1 Effect of Gelation Time

For quadruple batch synthesis, the reactant ratio was fixed at $4(SiO_2{:}\ 0.1Al_2O_3{:}\ 3K_2O{:}\ 410H_2O)$ and the temperature of 150°C. Figure 4.15 demonstrates the XRD patterns of quadruple batch synthesized products from different gelation times. It discloses that KH zeolite can be synthesized by gelling the sol-gel mixture for 19 hrs. However, when the gel was aged for a longer time (48 hrs), the XRD pattern reveals a surprise result since the diffraction pattern was

broader than that was gelled for 19 hrs. This result indicates that too much gelation time also has a negative effect on the crystallinity of KH zeolite under this synthesized conditions.

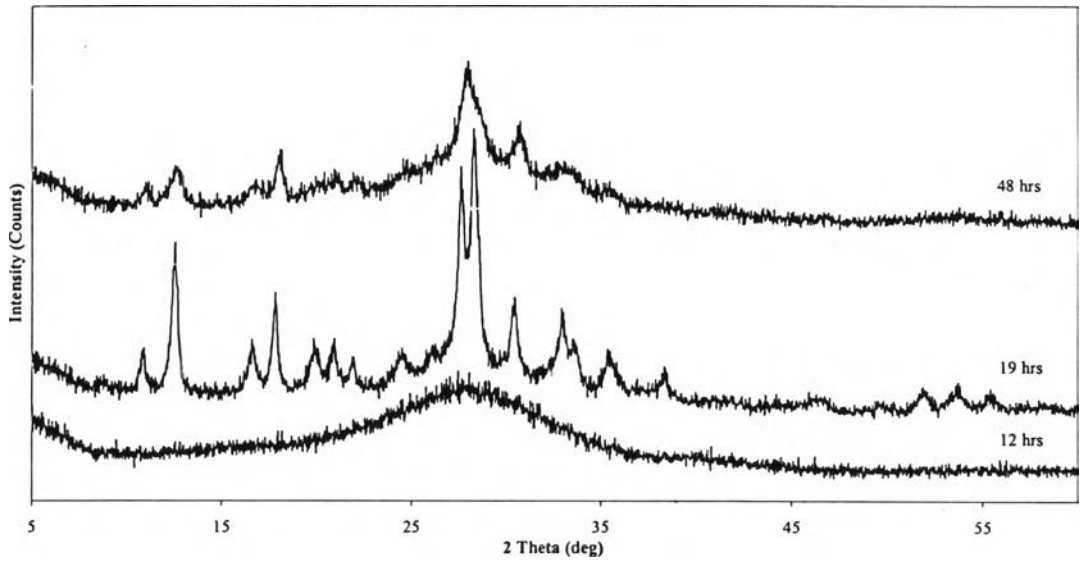

Figure 4.15 XRD patterns of quadruple batch synthesized products from $4(SiO_2{:}0.1Al_2O_3{:}3K_2O{:}410H_2O)$ at hydrothermal conditions 150°C and 5 hrs with 12, 19 and 48 hrs of gelation time.

The SEM micrographs of synthesized products from different gelation times as shown in Figure 4.16 also disclose a good agreement about zeolite morphology with XRD results. The dog-bone KH zeolite was only observed at 19 hrs of gelation time. Therefore, gellation of 19 hrs was suggested to be the appropriate time for quadruple batch synthesis. By using these particular conditions, the maximum yield of obtained KH zeolite was increased to around 0.4 g.

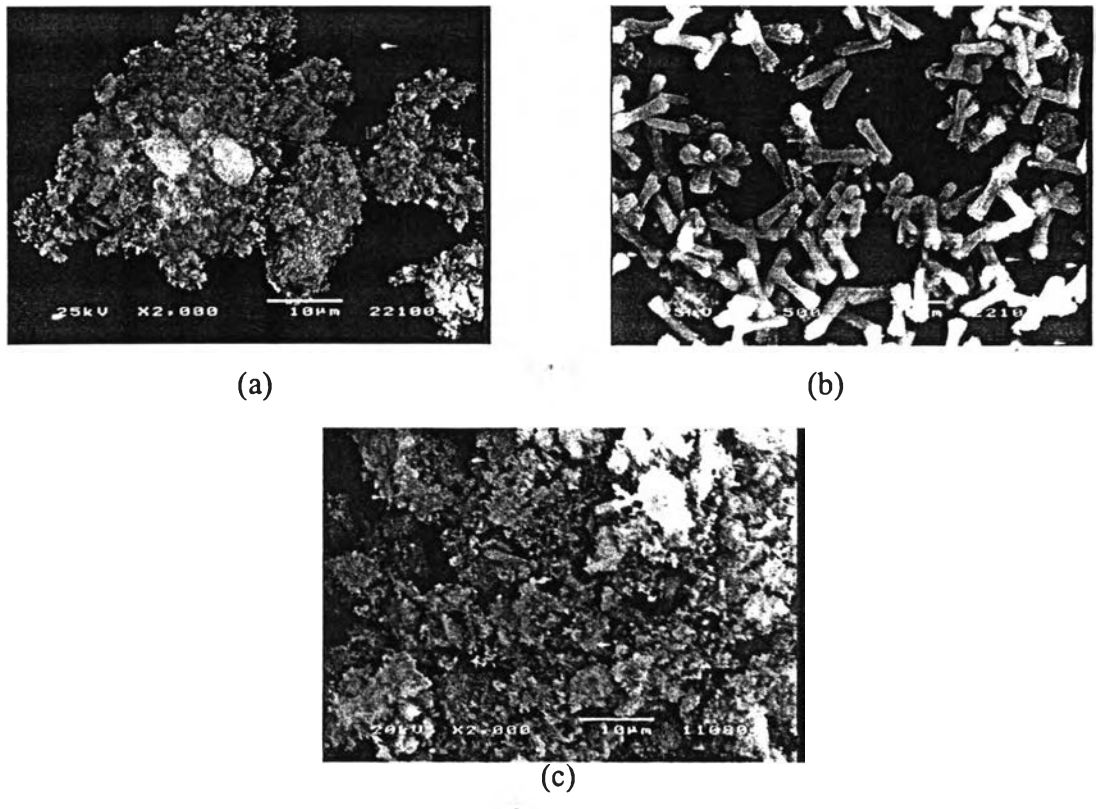

Figure 4.16 SEM micrographs of quadruple batch synthesized products from $3(SiO_2{:}0.1Al_2O_3{:}\ 3K_2O{:}410H_2O)$ at hydrothermal conditions 150°C, 5 hrs and gelling time of (a) 12, (b) 19 and (c) 48 hrs.

4.3 Catalytic Activity

4.3.1 Effect of KH Zeolite Morphology

Three different morphologies of synthesized KH zeolites were selected to study the effect of morphology on the catalytic activity for CH_4 reforming with CO_2 reaction. Eight percent of Ni was loaded onto flower-shape, dog-bone and disordered KH zeolites by using incipient wetness impregnation method. The activity testing was performed under 700°C for 5 hrs. The activity results are shown in Figures 4.17.

As depicted in Figure 4.17 it was revealed that all synthesized KH zeolites can give a very high activity on both CH_4 and CO_2 conversion. No

significant difference in CO_2 activity was observed for all Ni supported on three different morphologies KH zeolite along testing time. However, the CH_4 conversion of Ni supported on disordered KH zeolite seemed to be lower than those of Ni supported on the other two KH zeolites. In other words, Ni/flower-shape KH and Ni/dog-bone KH did not give a different activity to convert both CH_4 and CO_2 to CO and H_2. This result might be explained by the fact that the flower-shape morphology is destroyed by the grinding force during catalyst preparation, and each petal of the flower becomes isolatable presented as a dog-bone. Therefore, there are no different in catalytic activity whether Ni was supported on flower-shape or dog-bone KH, but the activity was slightly depressed when Ni was supported on disordered KH especially H_2 production.

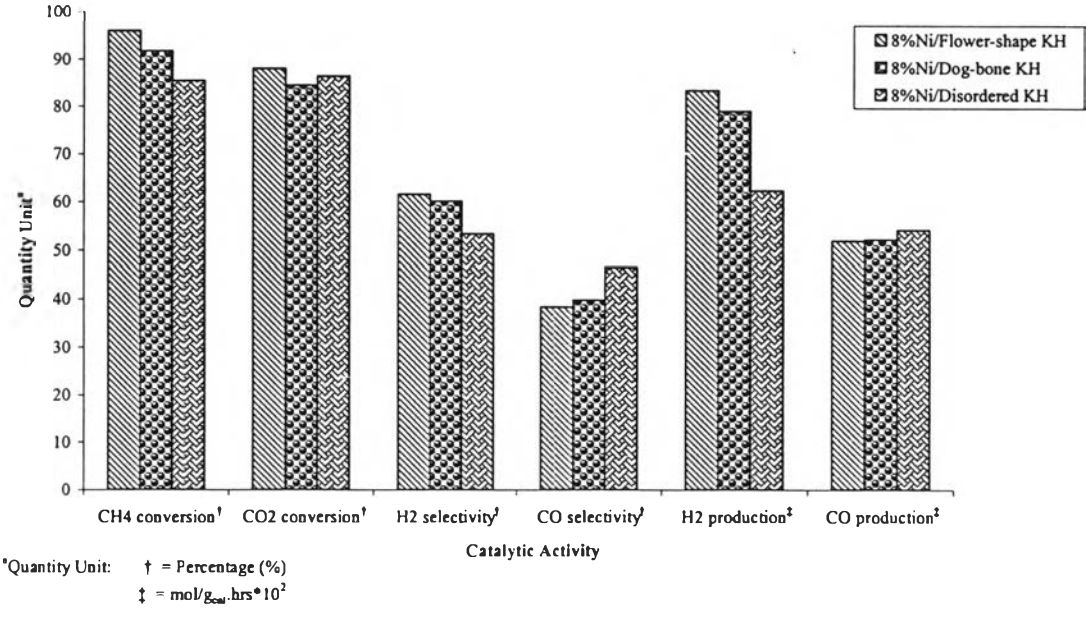

Figure 4.17 Effect of KH zeolite morphology on catalytic activity.

The results of H_2 selectivity and H_2 production also followed the trend of CH_4 conversion since a major of H_2 was produced by methane dissociation. For CO selectivity, higher percentage was observed for Ni/disordered KH, however, it provided low H_2/CO ratio as shown in Table 4.3.

Table 4.3 H_2/CO ratio produced from the three Ni supported on different morphology KH zeolites

Used Catalyst Name	H_2/CO Ratio
8%Ni/flower-shape KH	1.58
8%Ni/dog-bone KH	1.50
8%Ni/disordered KH	1.18

Table 4.3 shows H_2/CO ratio produced from the three Ni supported on different morphology KH zeolites. Theoretical H_2/CO ratio calculated from CH_4 reforming with CO_2 is one. For Ni/flower-shape KH and Ni/dog-bone KH, it was obviously found that both catalysts can provide a higher ratio of H_2/CO than one with the same quantity. On the other hand, Ni/disordered KH gave a lower H_2/CO ratio, which means the less profit on H_2 production. Therefore, it can be concluded that the morphology can affect CH_4 reforming activity and flower-shape or dog-bone KH are suggested to be the suitable supports for this reaction, since it can give the higher CH_4 conversion, and H_2 production.

4.3.2 Effect of Upscale Synthesis

KH zeolite synthesized from different batch scales were employed to be a support of 8%Ni catalysts. The activity testing was also performed under the same conditions as the previous experiments and the results are shown in Figure 4.18. For double batch and quadruple batch scale synthesized KH zeolites, almost identical activities were observed. By contrary, slightly lower in CH_4 conversion, H_2 selectivity and H_2 production were exhibited by KH zeolite synthesized from triple batch scale. This result can be explained by the morphology distinguishment of the triple batch scale KH zeolite.

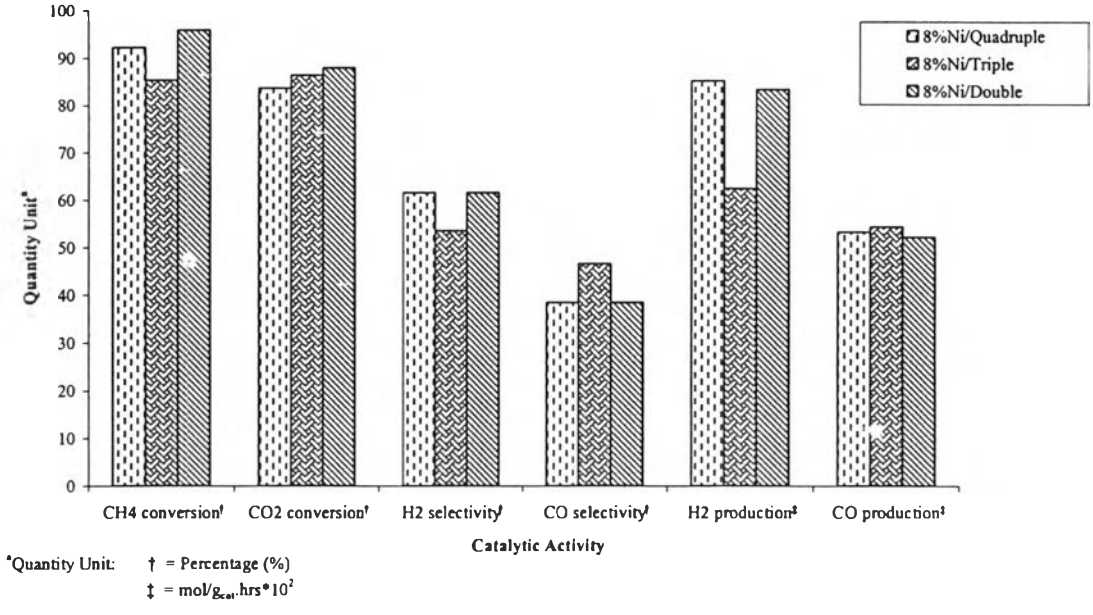

Figure 4.18 Effect of up-scaling on the catalytic activity.

As previously discussed, the disorder morphology of triple batch scale KH zeolite might depress the activity of the catalyst compared to that of the flower-shape or dog-bone of double batch and quadruple batch scales. Moreover, the H_2/CO ratio of triple batch scale KH zeolite is much lower than the other two. Therefore, flower-shape and dog-bone synthesized KH zeolite from quadruple batch scale synthesis is preferably to be a catalyst support for this reaction because it can be synthesized in the higher amount and with the higher activity to facilitate H_2 production.

4.3.3 Comparison of KH Zeolite with γ-Alumina Support

Synthesized KH zeolite and γ-Alumina, which is a commercial support for catalysis, were investigated on the CH_4 reforming activity. After loading with 8%Ni by incipient wetness impregnation method, both catalysts were tested for their activity under the same conditions as previously mentioned.

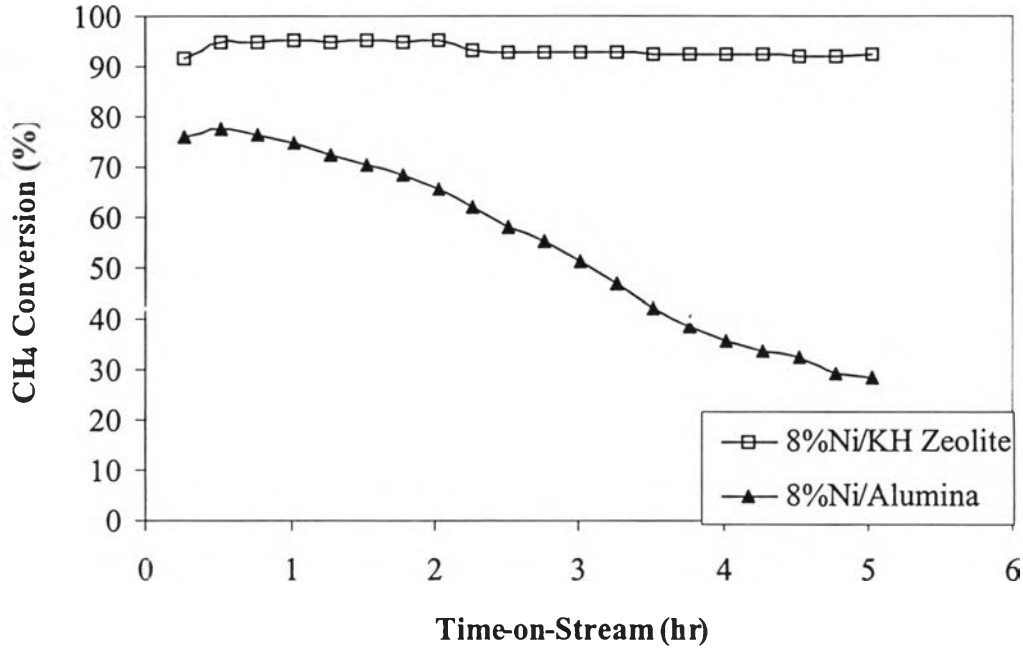

Figure 4.19 CH_4 conversion of 8%Ni supported on KH zeolite and 8%Ni supported on alumina.

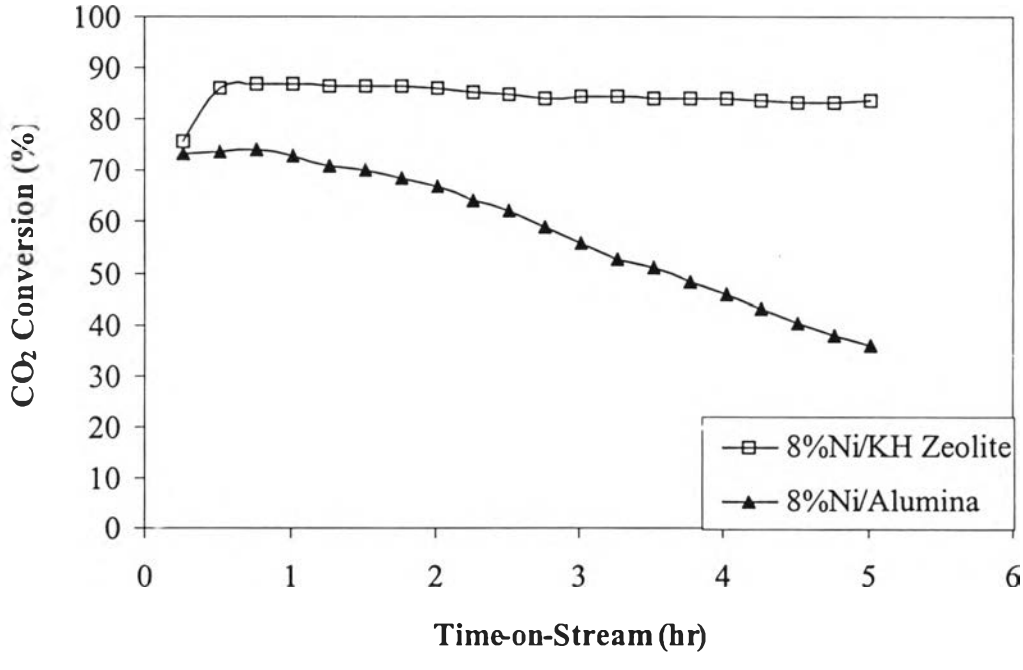

Figure 4.20 CO_2 conversion of 8%Ni supported on KH zeolite and 8%Ni supported on alumina.

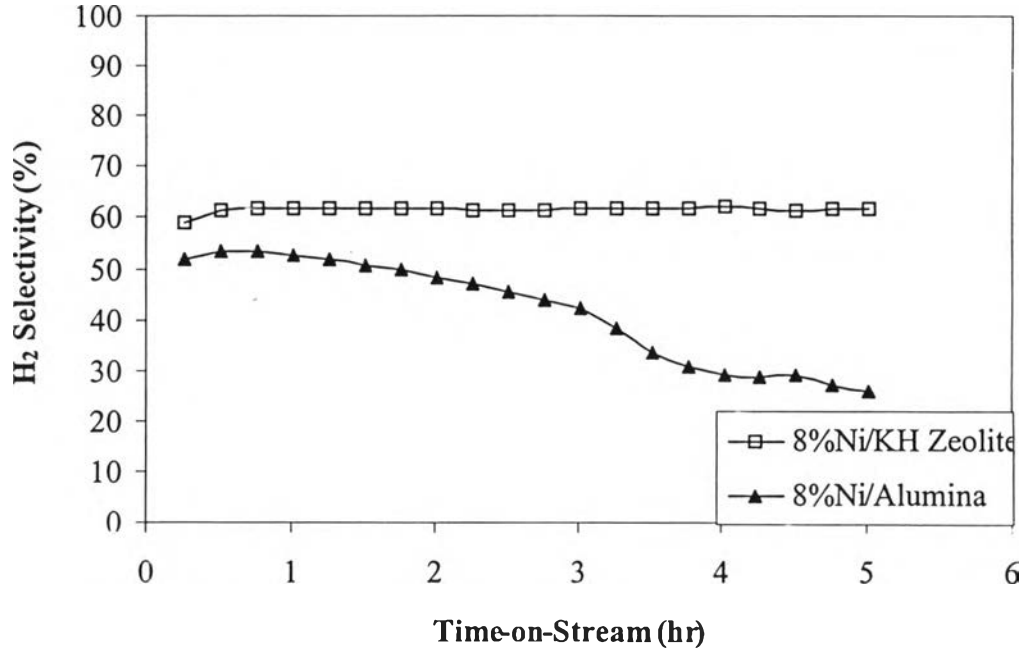

Figure 4.21 H_2 selectivity of 8%Ni supported on KH zeolite and 8%Ni supported on alumina.

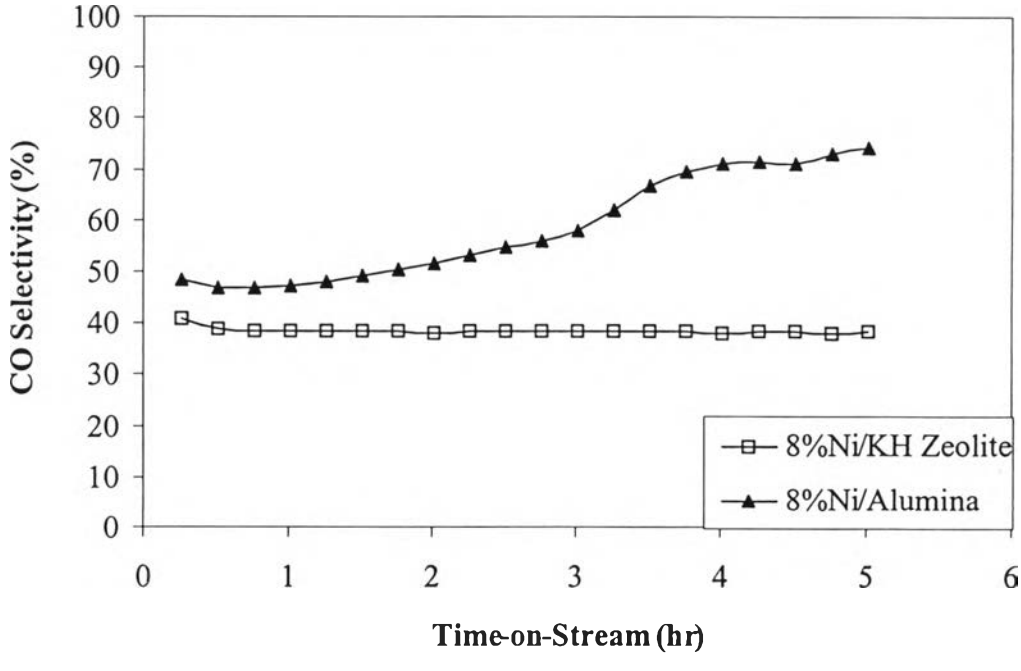

Figure 4.22 CO selectivity of 8%Ni supported on KH zeolite and 8%Ni supported on alumina.

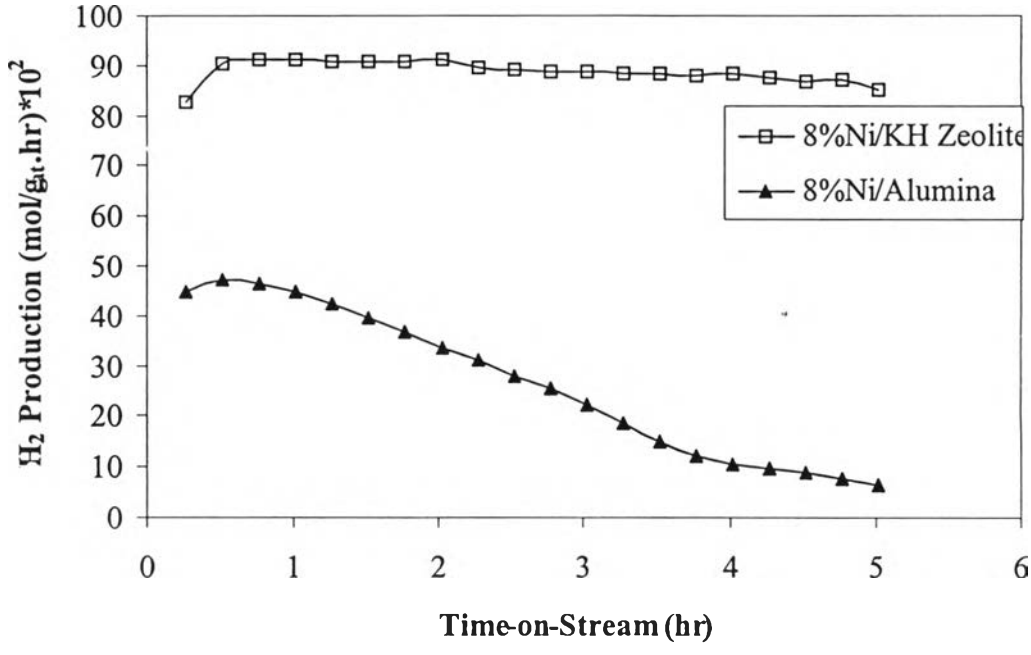

Figure 4.23 H_2 production of 8%Ni supported on KH zeolite and 8%Ni supported on alumina.

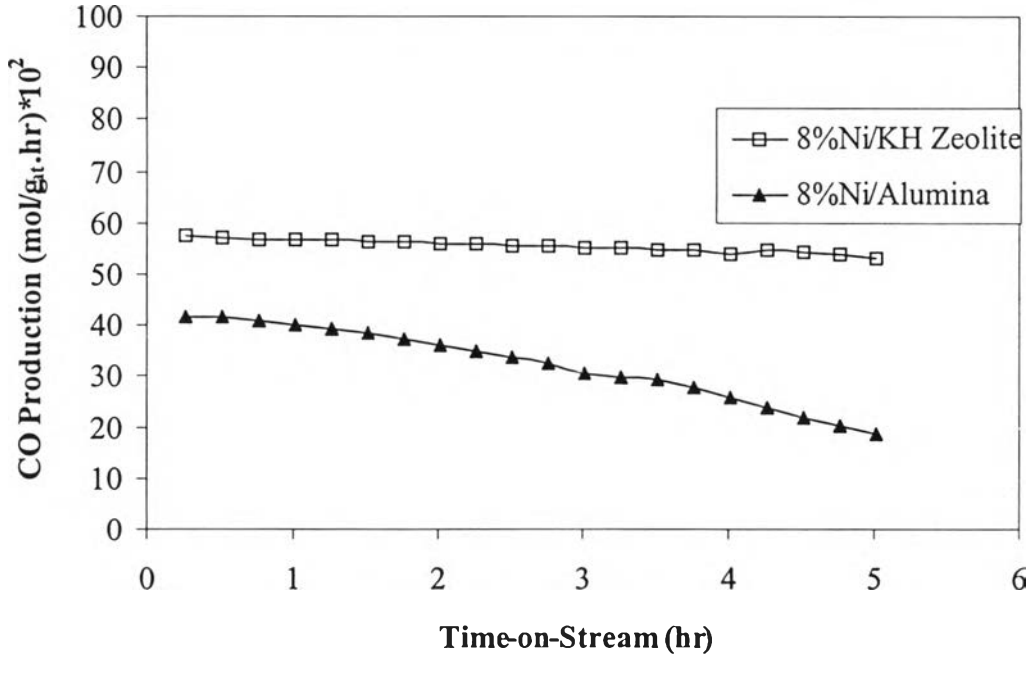

Figure 4.24 CO production of 8%Ni supported on KH zeolite and 8%Ni supported on alumina.

Figures 4.19 to 4.24 show all activity results of both employed Ni supported catalysts. It was found that Ni supported on synthesized KH zeolite provided an excellent activity on CH_4 and CO_2 conversions. Moreover, its activity tended to quite constant along testing time, which means that the synthesized KH zeolite showed the more stability than γ-Alumina. On the other hand, Ni supported on γ-Alumina catalyst showed a poorer activity and stability on both CH_4 and CO_2 conversions. Its initial activity was significantly lower than Ni supported on KH zeolite and dramatically decreased as the time on stream increased.

For H_2 and CO selectivity, the Ni/γ-Alumina catalyst initially provided H_2 and CO selectivity around 50% and its H_2 selectivity also dramatically decreased along time on stream. This result reveals that the Ni/γ-Alumina catalyst initially facilitated reforming reaction. Furthermore, the H_2 and CO production results of this catalyst also confirm the previous explanation. Since the conversion of both CH_4 and CO_2 decreased, all H_2 and CO production were also decreased, but dramatically decreased for H_2 production as previously discussed.

Since the synthesized KH in this study illustrated very high activity and also stability therefore; it was suggested to be the best and very excellent support for H_2 production. Moreover, the Ni/synthesized KH zeolite catalyst can provide the highest H_2/CO ratio compared to Ni/γ-Alumina catalyst, as listed in Table 4.4.

Table 4.4 H_2/CO ratio produced from the Ni/synthesized KH zeolite and Ni/γ-Alumina catalyst.

Used Catalyst Name	H_2/CO Ratio
8%Ni/KH zeolite	1.60
8%Ni/Alumina	0.82

4.3.4 Stability of KH Zeolite as Compared to Clinoptiolite's

Thermal stability of catalyst is the most important parameter for catalyst screening for appropriate applications or reactions. Moreover, the carbon dioxide reforming of methane is a reaction that requires high thermal stability

catalyst for the prevention of carbon deposition. Therefore, thermal stability of Ni/KH zeolite catalyst should be compared to other support; such as, Clinoptiolite which is the natural zeolite having high affinity for carbon dioxide (Nimwattanakul, *et al.*, 2005 *(In Press)*, Chang *et al.*, 2000). Eight percent of Ni was loaded on both KH zeolite and Clinoptiolite by using incipient wetness impregnation method. Furthermore, the addition of Zr promoter to 8%Ni/Clinoptilolite was employed to enhance the catalytic stability. The activity testing was performed under 700°C for 65 hrs. A comparative study of 8%Ni/KH zeolite and 8%Ni-2%Zr/Clinoptiolite was shown in Figures 4.25 to 4.30.

Surprisingly, the 8%Ni/KH zeolite showed much higher outcomes than the 8%Ni-2%Zr/Clinoptiolite in terms of CH_4 and CO_2 conversions, H_2 and CO productions and H_2 selectivity except only CO selectivity. All tendency of the 8%Ni-2%Zr/Clinoptiolite and the 8%Ni/KH zeolite catalyst were quite constant with increasing time on stream however, the 8%Ni/KH zeolite catalyst provided an excellent H_2 production. Therefore, it is clear that the synthesized KH zeolite becomes a promising support for CH_4 reforming with CO_2 since, it gave the higher H_2 production and catalytic stability.

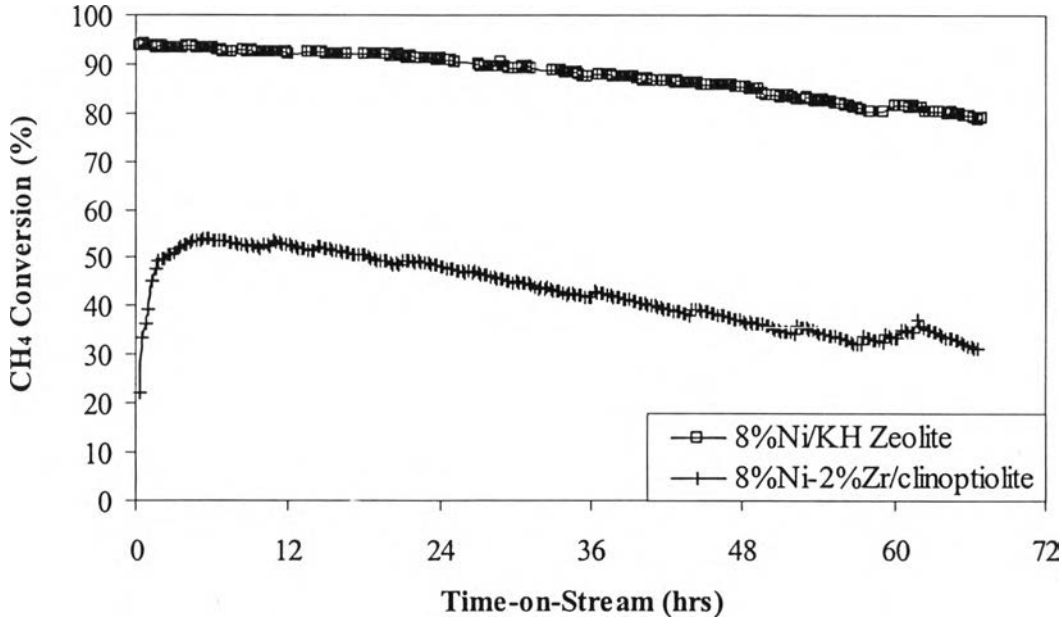

Figure 4.25 CH_4 conversion of 8%Ni supported on KH zeolite and 8%Ni-2%Zr supported on Clinoptiolite.

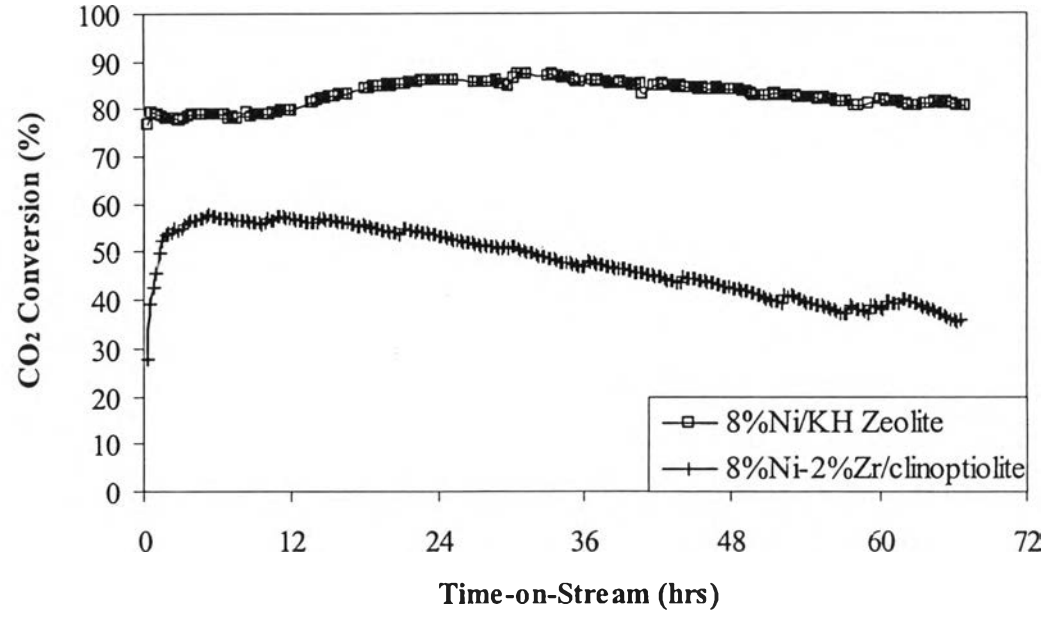

Figure 4.26 CO_2 conversion of 8%Ni supported on KH zeolite and 8%Ni-2%Zr supported on Clinoptiolite.

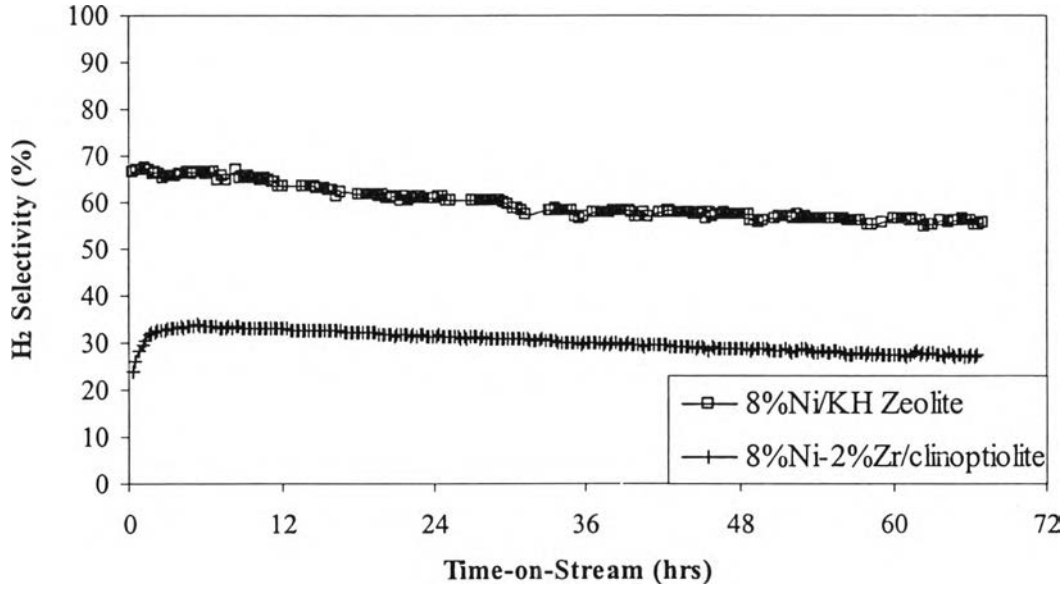

Figure 4.27 H_2 selectivity of 8%Ni supported on KH zeolite and 8%Ni-2%Zr supported on Clinoptiolite.

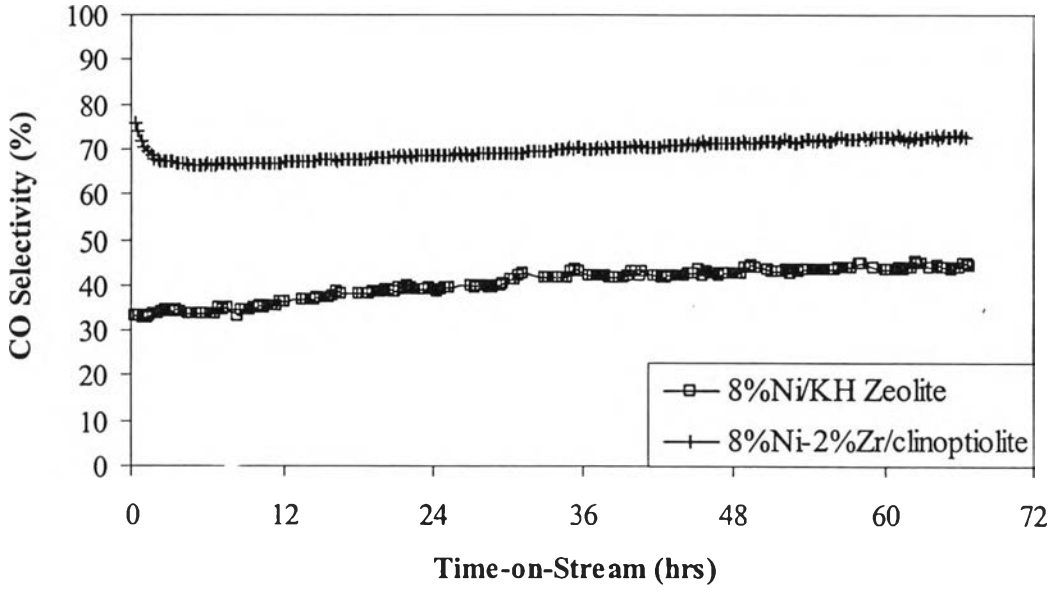

Figure 4.28 CO selectivity of 8%Ni supported on KH zeolite and 8%Ni-2%Zr supported on Clinoptiolite.

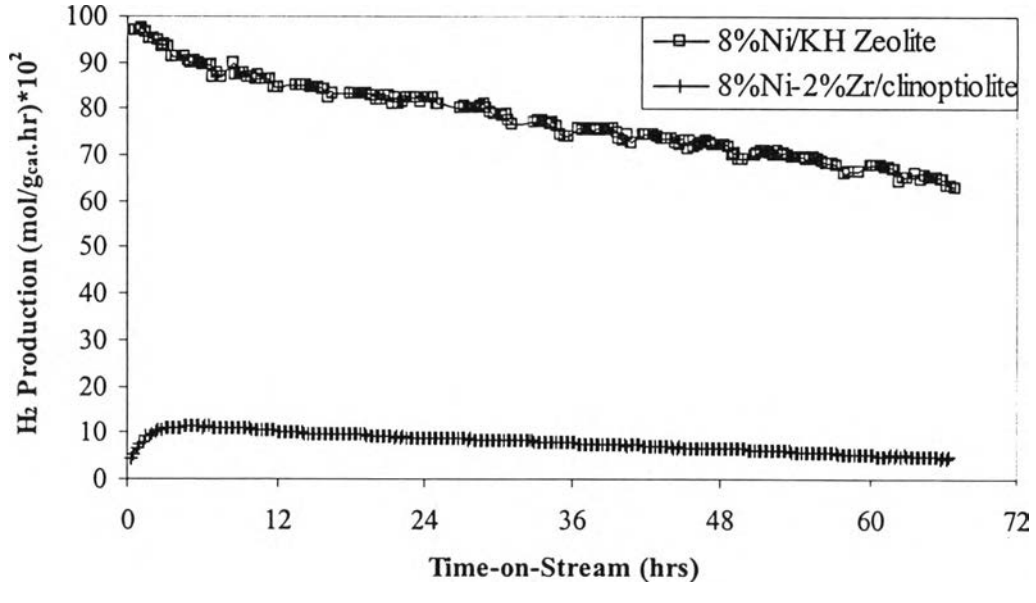

Figure 4.29 H_2 production of 8%Ni supported on KH zeolite and 8%Ni-2%Zr supported on Clinoptiolite.

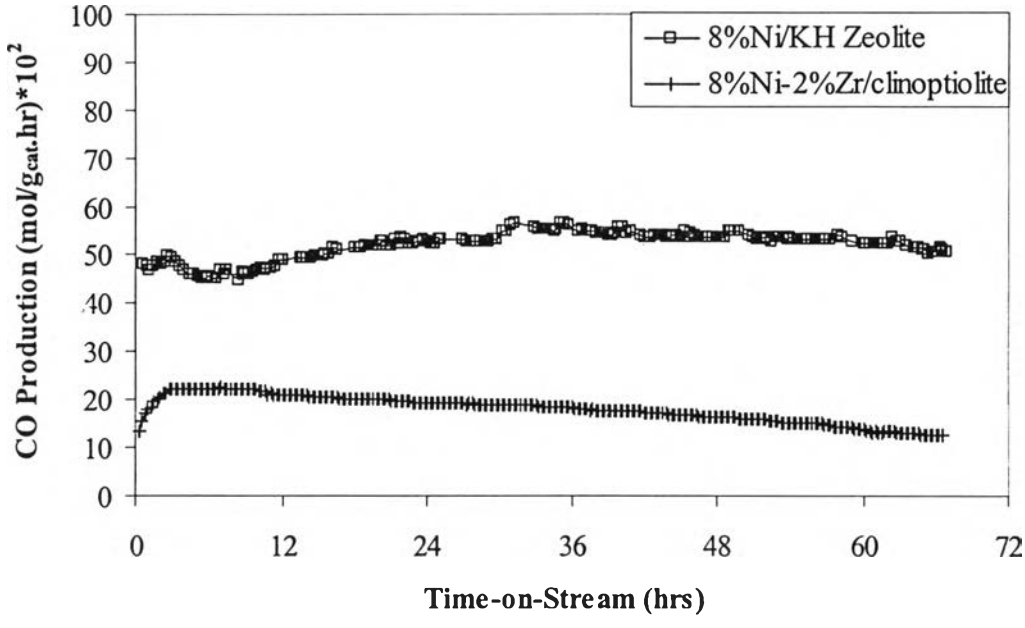

Figure 4.30 CO production of 8%Ni supported on KH zeolite and 8%Ni-2%Zr supported on Clinoptiolite.

4.4 Catalysts Characterizations

4.4.1 Thermogravimetric Analysis

Coke formation in the CO_2 reforming of CH_4 is generally known to cause the catalyst deactivation as previously shown. It has been mainly focus on CH_4 cracking and Boudouard reaction. Thermogravimetric Analysis (TGA) was employed to estimate the amount of carbon deposition that generally occurs with dry reforming reaction on the used catalysts. The amount of coke from TGA results was shown in Figures 4.31, 4.33 and 4.34.

In Figure 4.31, it was found that the carbon deposition on used 8%Ni supported on flower-shape and dog-bone KH catalysts were lower than that on the used 8%Ni supported on disordered KH. It can be obviously seen that the coke deposition and CO_2 conversion disclosed the similar trend. This might be explained that the formation of coke might take place via the CO disproportional reaction (Boudouard Reaction) instead of CH_4 decomposition because the coke deposition

showed the different trend compared to CH_4 conversion as shown in the equation below.

$$2CO_{(g)} \longrightarrow C_{(s)} + CO_{2(g)} \qquad (4.1)$$

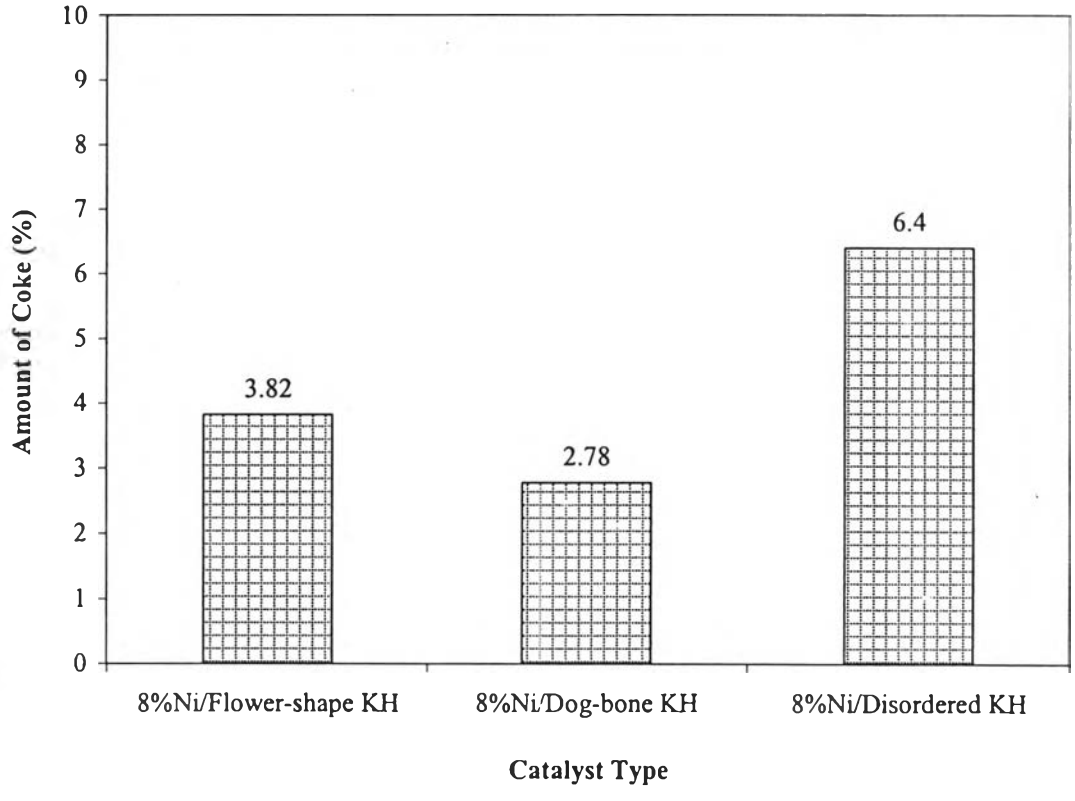

Figure 4.31 Amount of coke on used catalyst with effect of morphology.

Therefore, the reaction mechanism is proposed that CH_4 are initially decomposed into $C_{(s)}$ (carbon atom), and two moles of H_2 as exhibited in reaction [1] in Figure 4.32 (Stagg and Resasco, 1998). Subsequently, CO_2 in the feed will react $C_{(s)}$ to produce two moles of CO by reaction [2]. Two moles of the produced CO is further disproportionate to reproduce CO_2 and additional $C_{(s)}$; reaction [3]. Besides, if there is no further reaction involved in the mechanism, the CO_2 conversion should be low. From the experiment, the observed CO_2 conversion was rather high as shown in the previous section. Therefore, it is proposed that CO_2 is further reacted with H_2 to form CO and H_2O known as the reversed water gas shift reaction; reaction [4]. Nevertheless, H_2/CO ratio was greater than one. This means that the water gas shift reaction slightly takes place in the reaction; reaction [5].

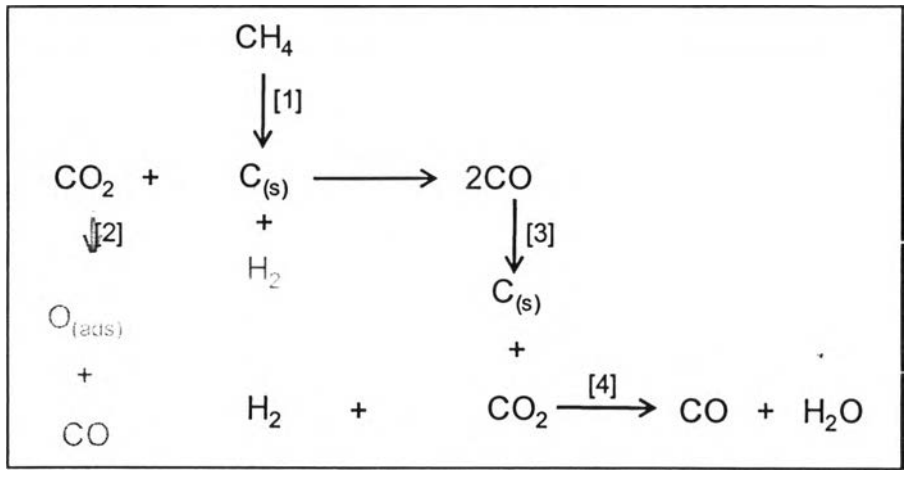

Figure 4.32 Possible mechanism proposed for the relationship between CO_2 conversion and coke formation.

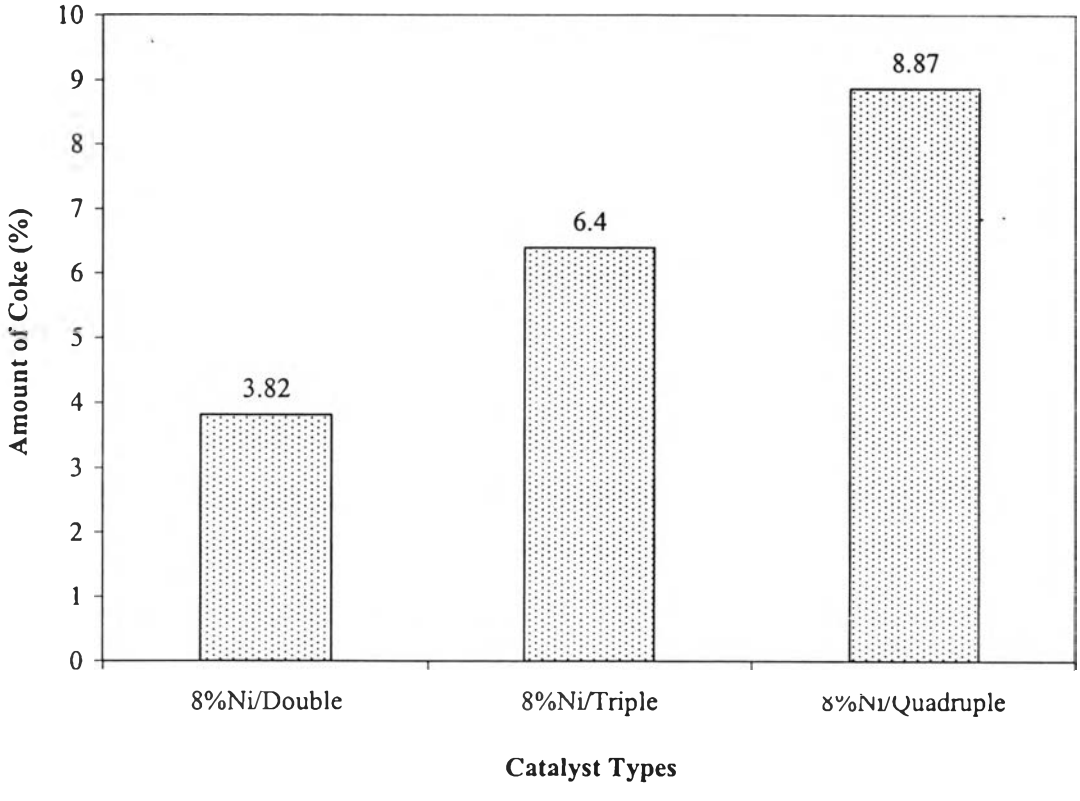

Figure 4.33 Amount of coke on used catalyst with effect of upscaling.

Besides, Figure 4.33 exhibits that the carbon deposition of used Ni-supported on KH zeolite synthesized from different batch scales increased with increasing scale number of KH zeolite synthesis. The TGA results indicated that the

used 8%Ni/Quadruple showed the highest amount of coke after 5 hrs of reaction. However, its activity did not depress along testing time, and was also quite similar to that of 8%Ni/Double batch scale catalyst even their coke deposition quantity was significantly different. This may be concluded that the activity of KH zeolite is independent on the coke deposition. The results also reveal that the coke deposition on the used catalysts showed the same tendency as CO_2 conversion due to the reaction mechanism proposed earlier.

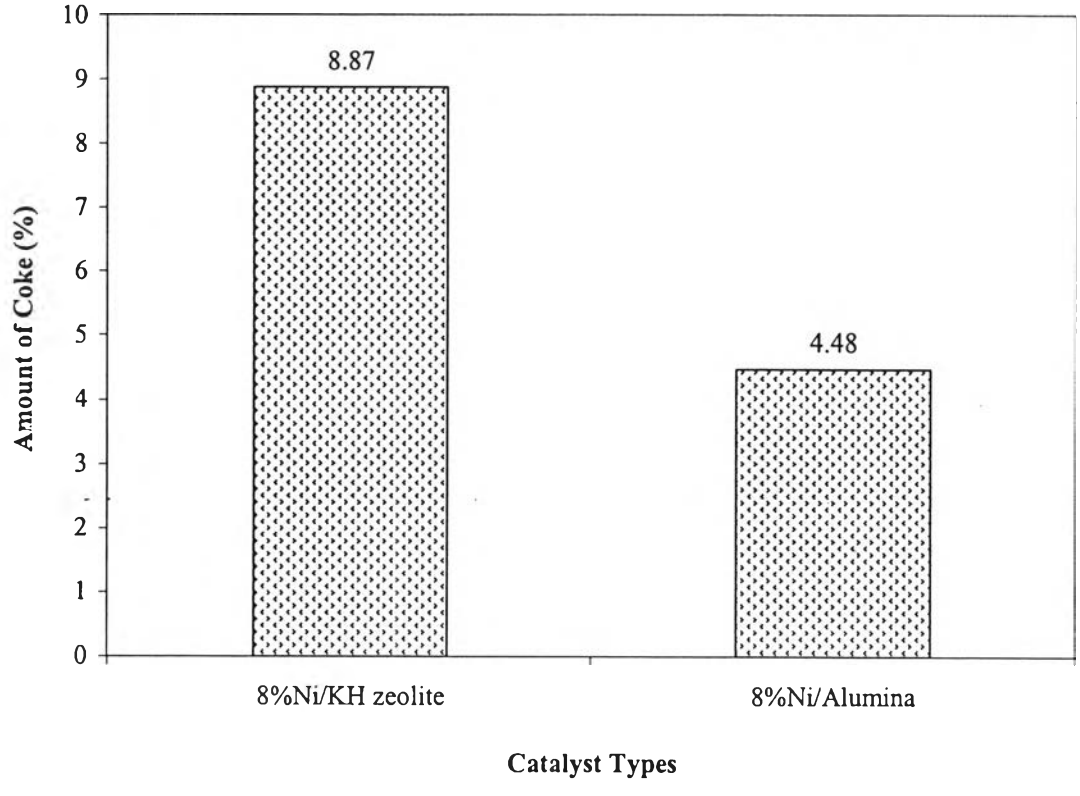

Figure 4.34 Amount of coke on used 8%Ni/KH zeolite and 8%Ni/Alumina catalyst.

Since the H_2 production on Ni/γ-alumina was initially greater but it gradually decreased with increasing time on stream. This may be because suddenly CH_4 decomposition within the first hour of the reaction causes the coke formation on the active site for the decomposition of CH_4 leading to low H_2 production. However, the lower coke deposition was clearly observed for Ni/γ-alumina, as shown in Figure 4.34, since the catalyst has a gradually low activity to decompose methane as mentioned earlier.